

A new analysis of fine-structure constant measurements and modelling errors from quasar absorption lines

Michael. R. Wilczynska,^{1*} John K. Webb,^{1†} Julian A. King,¹

Michael T. Murphy,² Matthew B. Bainbridge,¹ and Victor V. Flambaum,¹

¹*School of Physics, University of New South Wales, Sydney, NSW 2052, Australia*

²*Centre for Astrophysics and Supercomputing, Swinburne University of Technology, Victoria 3122, Australia*

Released 2014 Xxxxx XX

ABSTRACT

We present an analysis of 23 absorption systems along the lines of sight towards 18 quasars in the redshift range of $0.4 \leq z_{abs} \leq 2.3$ observed on the Very Large Telescope (VLT) using the Ultraviolet and Visual Echelle Spectrograph (UVES). Considering both statistical and systematic error contributions we find a robust estimate of the weighted mean deviation of the fine-structure constant from its current, laboratory value of $\Delta\alpha/\alpha = (0.22 \pm 0.23) \times 10^{-5}$, consistent with the dipole variation reported in Webb et al. (2011) and King et al. (2012).

This paper also examines modelling methodologies and systematic effects. In particular we focus on the consequences of fitting quasar absorption systems with too few absorbing components and of selectively fitting only the stronger components in an absorption complex. We show that using insufficient continuum regions around an absorption complex causes a significant increase in the scatter of a sample of $\Delta\alpha/\alpha$ measurements, thus unnecessarily reducing the overall precision. We further show that fitting absorption systems with too few velocity components also results in a significant increase in the scatter of $\Delta\alpha/\alpha$ measurements, and in addition causes $\Delta\alpha/\alpha$ error estimates to be systematically underestimated. These results thus identify some of the potential pitfalls in analysis techniques and provide a guide for future analyses.

Key words: atomic data – line: profiles – methods: data analysis – techniques: spectroscopic – quasars: absorption lines

1 INTRODUCTION

Modern physical theories utilise a set of fundamental constants. These constants are defined as dimensionless ratios of physical quantities and have no dependence on other measured parameters. As such, it is important to know the numerical values of these constants to high accuracy. Weyl (1919), Eddington (1931) and Dirac (1937) were amongst the first to investigate the possibility that these fundamental constants may vary with time. More recently, attempts at deriving unifying theories of nature have revived interest in varying constants, as some of these theories predict the variation of fundamental constants. For a comprehensive review of both theory and observations see Uzan (2011). This

work focuses on the fine-structure constant $\alpha \equiv e^2/4\pi\epsilon_0\hbar c$ and its possible variation:

$$\Delta\alpha/\alpha \equiv \frac{\alpha_z - \alpha_0}{\alpha_0}, \quad (1)$$

comparing the laboratory value, α_0 , with the value at some redshift, α_z .

Quasar absorption line systems provide important probes of the possible variation of the fine-structure constant over cosmological time-scales and distances. These analyses exploit the absorption features caused by intervening gas clouds along the lines of sight to background quasars. Possible evidence for a varying α has surfaced in recent years. These studies employed the ‘Many-Multiplet’ (MM) method (Dzuba et al. 1999; Webb et al. 1999), beginning with 30 absorption systems observed on the Keck telescope (Webb et al. 1999) and later extended to 140 absorption systems by Murphy et al. (2003) and Murphy et al.

* E-mail: mikew@phys.unsw.edu.au

† E-mail: jkw@phys.unsw.edu.au

(2004). The next large study used observations from the Very Large Telescope (VLT) consisting of 154 measurements of α (King et al. 2012). Combining the results of the Keck sample with those of the VLT sample, Webb et al. (2011) and King et al. (2012) found that the data indicated a variation in α across the sky that could be consistently modelled with a spatial dipole. If correct, clearly the result is of fundamental significance and hence must be critically tested and the associated systematic effects comprehensively understood.

The quasar absorption system sample investigated in this work has been previously studied, with a discussion arising in the literature about the validity of the analysis (Chand et al. 2004; Murphy et al. 2007; Srianand et al. 2007; Murphy et al. 2008). We present an independent analysis of this sample of quasar absorption systems.

This work will examine, in greater detail compared to previous work, methodologies associated with absorption line modelling techniques. To explore the systematic effects of differing fitting methods on $\Delta\alpha/\alpha$ measurements we model the 23 absorption systems in three different ways. We also discuss how different analysis strategies can significantly influence uncertainties in measurements of a fractional change in α .

We choose to work with this sample of absorbers, originally analysed by Chand et al. (2004) (hereafter C04), for a variety of reasons: the absorption systems within this sample have relatively simple velocity structures; the sample is large enough such that meaningful statistical analysis may be applied to gain insight into the effects of differing fitting methodologies; and finally, this sample has been previously studied thereby allowing for a comparison of previous results with the independent analysis of this work.

A potentially important source of systematic errors in modelling quasar absorption systems to derive estimates of space-time variation of α concerns possible spectral wavelength distortions. Griest et al. (2010) first discovered small-scale, i.e. intra-order, wavelength calibration problems. Molaro et al. (2008) first searched for possible wavelength distortions across echelle orders by comparisons with echelle calibrations from asteroids measurements. Rahmani et al. (2013) subsequently discovered large-scale, approximately linear distortion effects and a more detailed study was carried out by Evans et al. (2014). Evans et al. (2014) compared observations from different telescopes of the same quasar and found long range distortions of the quasar spectra's wavelength scales. Recently Whitmore & Murphy (2015) applied a simple distortion model to quasar simulations and concluded that long range wavelength distortions are capable of significantly weakening the evidence for variations in α from quasar absorption lines. We note that the Whitmore & Murphy (2015) model effectively assumes a single-wavelength setting, inappropriate for most quasar observations. This assumption is critically examined in a parallel study (Dumont & Webb 2016) who reach different conclusions and we therefore do not include distortion models presented in Whitmore & Murphy (2015).

1.1 Overview

In Section 2, we describe the spectroscopic and atomic data used in our analysis. Section 3 describes the profile analy-

sis methods used in this work. Section 4 describes the Least Trimmed Squares (LTS) Method, which is used to estimate a random, systematic error we incorporate into our final results. Section 5 presents our methodology for and our independent analysis of the dataset. Section 6 describes two additional fitting methodologies we apply to the entire dataset and the quantitative effects of applying differing Voigt profile fitting methodologies on measurements of $\Delta\alpha/\alpha$.

2 SPECTROSCOPIC AND ATOMIC DATA

The raw spectroscopic data we use in this work is the same as presented in Chand et al. (2004). However, we have independently reduced the raw spectra to produce the 1-dimensional calibrated spectra as described below. We have not included any additional data other than that used in Chand et al. (2004). All spectral data are taken from the VLT/UVES archive. Raw spectra were reduced to 1-dimensional format and calibrated using the MIDAS pipeline, provided by ESO. We have used the updated echelle spectrograph ThAr line list detailed in Murphy et al. (2007). We have followed the same procedures for these and all other aspects of data reduction and calibration, as described in King et al. (2012).

The MIDAS extraction routine incorrectly estimates the spectral errors associated with the flux of data points in the base of saturated absorption lines. When individual exposures are combined UVES_POPLER¹ provides a check on the concordance between the different exposures. UVES_POPLER calculates the value of χ^2_ν for each combined flux pixel by considering the dispersion of the contributing pixels from each exposure about their weighted mean. The bases of saturated lines typically produce a $\chi^2_\nu \geq 2$, suggesting that MIDAS spectral error arrays underestimate the statistical uncertainty in those regions. The problem is more noticeable towards the blue end of spectra. The effect of this is to underestimate the statistical uncertainty on $\Delta\alpha/\alpha$ derived from these data points. To rectify this problem we adjust the error arrays to account for the inconsistency present in our spectra (see Section 2.1 of King et al. (2012)).

q -coefficients of atomic transitions, which determine the sensitivity to α variation for a given atomic transition, wavelength ID's and ion codes used in this work are presented in Table 1. The atomic data in Table 1 are taken from Table B1 of King et al. (2012), although we use different ion codes. We make use of isotopic structure where available (relevant for Si II, Mg I, Mg II, Zn II in this work). We note that although there may be hints of a departure from terrestrial isotopic relative abundances for Mg at high redshift, we do not regard existing measurements as definitive. For this reason, and because the analysis in this paper focuses on systematics associated with two particular issues (under-fitting and restricted spectral fitting regions), we have carried out the modelling in this paper using terrestrial relative abundances throughout.

¹ http://astronomy.swin.edu.au/~mmurphy/UVES_popler/

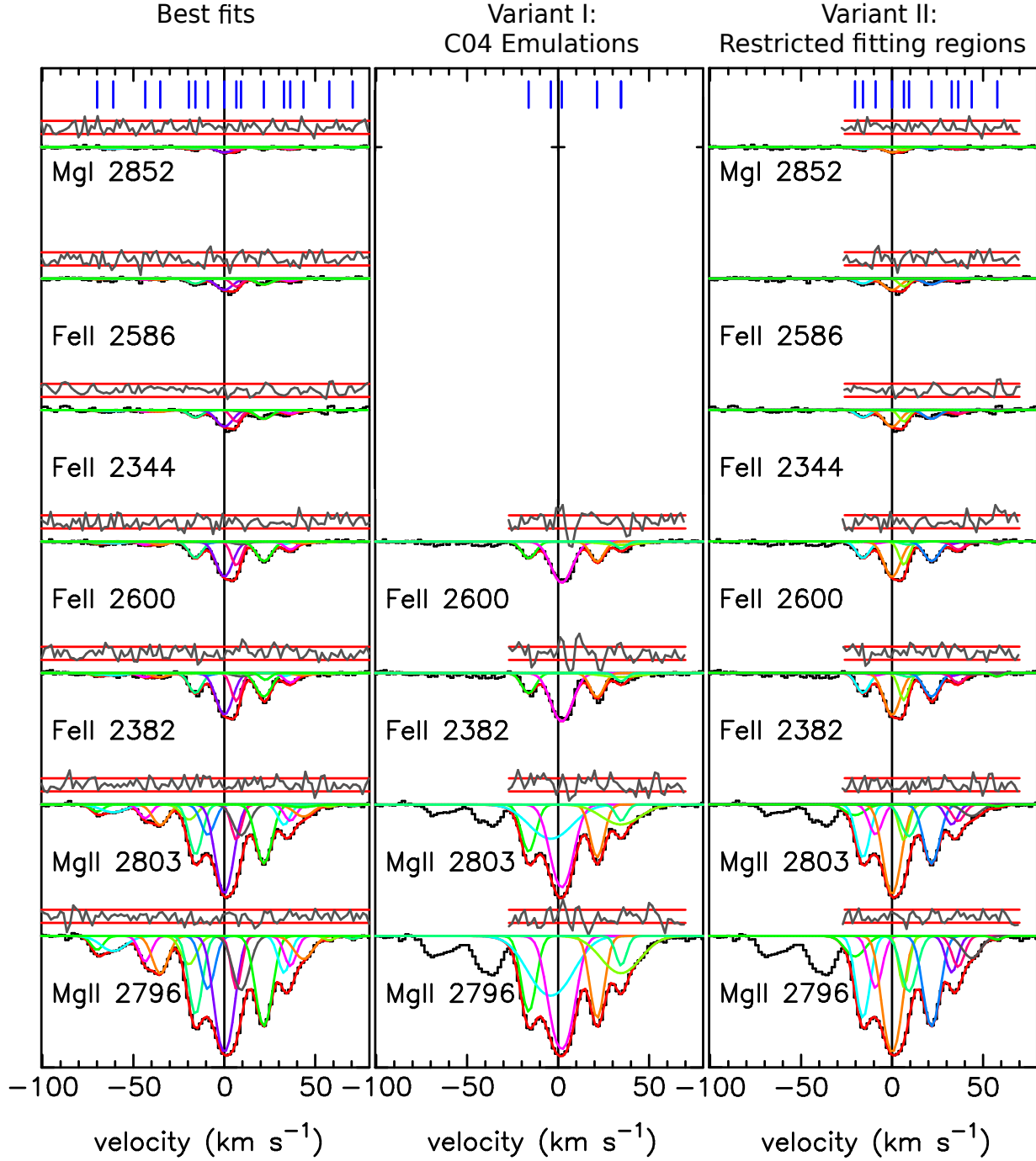


Figure 1. All three columns show $z_{abs} = 0.942$ absorption system along the line of sight to quasar J222006-280323. The first column shows our best fits to the data. The second column shows our C04 emulations (Variant I). The third column shows our best fits but with restricted fitting regions (Variant II). The models to the data are shown as red lines. The individual components are all plotted in different colours. Normalised residuals ($[\text{model} - \text{data}] / \text{error}$) are shown in grey between the horizontal red $\pm 1\sigma$ error lines. Blue tick marks indicate individual velocity components. The best fit give a result of $\Delta\alpha/\alpha = (0.686 \pm 1.130) \times 10^{-5}$, with a $\chi^2_\nu = 0.947$. Variant I gives a result of $\Delta\alpha/\alpha = (-1.400 \pm 0.508) \times 10^{-5}$, with a $\chi^2_\nu = 2.480$. Variant II gives a result of $\Delta\alpha/\alpha = (0.068 \pm 1.010) \times 10^{-5}$, with a $\chi^2_\nu = 1.009$. The normalised residuals illustrate the limits of the fitting regions. Two contaminants are present in our best fit. One weak, but warranted by AICc, contaminant in MgII $\lambda 2803$ at $v \approx 35 \text{ km s}^{-1}$ and another in FeII $\lambda 2383$ at $v \approx 18 \text{ km s}^{-1}$. Note the difference in fitting regions when comparing the Variant I system to that of our best fit. The fitting regions for Variant I extend only over the strongest absorption features, excluding absorption in the system that is clearly present. No continuum regions have been included for Variant I. Parameters describing the varying continuum and varying zero-level are not shown, but fitting parameters for all three models are provided in the supplementary material.

Table 1. Selected atomic data. Column 1 shows the common names of transitions. Wavelength ID's are provided in column 2. Actual wavelengths used in this work are compiled from isotopic structure, where available, and are taken from Table B1 of King et al. (2012) (also see Section 3). q -coefficients, which determine the sensitivity of atomic transitions to a change in α (Dzuba et al. 1999; Murphy et al. 2003), are given in column 3. The letters in column 4 offer a simple shorthand for labeling transitions used to fit absorption systems. Our codes differ from those in King et al. (2012) for clarity. King et al. (2012) provide a thorough compilation of atomic data used in this work.

Ion	λ_{ID}	$q[\text{cm}]^{-1}$	Code
Fe II	1608	−1300(300)	a_1
	2260	1435(150)	a_2
	2344	1210(150)	a_3
	2374	1590(150)	a_4
	2382	1460(150)	a_5
	2586	1490(150)	a_6
	2600	1330(150)	a_7
Mg I	2852	86(10)	b_1
Mg II	2796	211(10)	c_1
	2803	120(2)	c_2
Al II	1670	270(30)	d_1
Al III	1854	464(30)	e_1
	1862	216(30)	e_2
Si II	1526	50(30)	f_1
	1808	520(30)	f_2
Mn II	2576	1420(150)	g_1
	2594	1148(150)	g_2
	2606	986(150)	g_3
Ni II	1709	−20(250)	h_1
	1741	−1400(250)	h_2
Cr II	2056	−1110(150)	i_1
	2026	−1280(250)	i_2
	2066	−1360(250)	i_3
Zn II	2026	2479(25)	j_1
	2062	1584(25)	j_2

3 PROFILE ANALYSIS METHODS

In Sections 5 and 6 we use VPFIT² version 10.0 as our χ^2 minimization algorithm. VPFIT has been shown to be robust in its calculation of statistical uncertainties using Markov Chain Monte Carlo methods (King et al. 2009). The instrumental settings for the data used in this analysis, assuming a Gaussian instrumental profile, correspond to a FWHM of 6 km s^{−1}.

Estimates of α are derived using the Many Multiplet method (Dzuba et al. 1999; Webb et al. 1999), modelling all transitions simultaneously. Table 2 provides a key for identifying which transitions are used in each absorption system and model. $\Delta\alpha/\alpha$ is explicitly included as an additional free parameter which is varied along with all other parameters to minimize χ^2 .

All profile fits used in this work are made available in the supplementary material.

4 THE LEAST TRIMMED SQUARES (LTS) METHOD

Following King et al. (2012) (Section 3.5.3) we use a LTS procedure to explore the statistical properties of our whole dataset. That is, once we have measured $\Delta\alpha/\alpha$ in each absorber for each model we apply the LTS algorithm to the set of 23 $\Delta\alpha/\alpha$ measurements for each model. The purpose of applying the LTS method is twofold: to check whether there exist any outliers in the datasets; and, to determine an appropriate systematic error term to be added to each measurement of $\Delta\alpha/\alpha$ in quadrature. King et al. (2012) utilised a fast-LTS algorithm (Rousseeuw & Driessen 2006), which computes orders of magnitude faster for large data sets compared to an LTS algorithm that computes the exact LTS procedure. We use an exact LTS algorithm as our dataset is small enough to accommodate an exhaustive search. Applying the LTS method removes the impact of any anomalous data points and is likely to provide a more robust estimate of $\Delta\alpha/\alpha$. Individual error estimates on $\Delta\alpha/\alpha$ returned by VPFIT only account for the statistical properties of the spectral noise and do not account for unknown systematics. For that reason, we introduce an additional error component added in quadrature to the VPFIT error term such that $\sigma_{total}^2 = \sigma_{stat}^2 + \sigma_{rand}^2$. We use the LTS method to allow for the inclusion, and calculation, of σ_{rand} .

Instead of fitting n data points, the LTS method fits only $k = (n + p + 1)/2$ points (where p is the number of free parameters) using standard least-squares minimization and then searches for the combination of k data points and fitted model that yields the lowest sum of squared residuals. The method only fits the inner k/n fraction of the distribution of the residuals. Where up to $k - n$ outliers exist, they will be ignored in the calculation of σ_{rand} by this method provided they are in the excluded fraction (Rousseeuw 1984).

To summarise, the steps are as follows:

- (i) We select all possible subsets of n from k observations.
- (ii) For each combination we compute the weighted mean value of $\Delta\alpha/\alpha$, varying σ_{rand} in the quadrature error term such that the observed χ_ν^2 is equal to the expected value, given by Eq.17 in King et al. (2012). σ_{rand} is then determined in a more robust manner, without undue influence from anomalously deviant points, if any.
- (iii) Finally the σ_{rand} deemed to be applicable to the whole sample is selected as the smallest value out of all possible combinations. Selecting the smallest value of σ_{rand} ensures that its value is not overestimated by high scatter points and that any possible outliers are not ‘masked’ by an artificially inflated σ_{rand} . In this way we take into account, in a robust way, any possible systematic contribution to the overall error on $\Delta\alpha/\alpha$.
- (iv) After applying σ_{rand} to the entire dataset we search for any points with $|r_i| = |(\Delta\alpha/\alpha - \text{model prediction})/\sigma_{tot}| \geq 3$ as outliers. However, none were found in this analysis.

Note that for point (ii) above the LTS method increases σ_{rand} sufficiently enough to reduce χ_ν^2 to an expected value and not unity. The expected value of χ_ν^2 is lower than unity due to the fact that the sample in question is a trimmed subset (k/n) of the original sample. In this situation it is possible for a sample with a weighted mean giving χ_ν^2 of

² <http://www.ast.cam.ac.uk/~rfc/vpfit.html>

Table 2. Transitions used in all fits contributing to the determination of $\Delta\alpha/\alpha$. Columns 3 and 4 gives the quasar emission redshift and absorption redshift respectively. The key for transition labels in column 5 and 6 is given in Table 2. The b -parameters and redshifts for each component of an absorption system were tied in the fitting process for all species as described in Section 5.4, with the exception of AlIII. AlIII was fitted simultaneously, where available, but its b -parameters and redshifts were fitted independantly.

Quasar Name		Transitions			
J2000	B1950	z_{em}	z_{abs}	Best fits and Variant II	Variant I
J134427-103541	HE 1341-1020	2.35	0.873	$a_3a_4a_5b_1c_1c_2$	$a_3a_5a_6b_1c_1c_2$
J134427-103541	HE 1341-1020	2.35	1.278	$a_2a_3a_4a_7b_1c_1c_2g_1g_3$	$a_3a_4a_5a_7c_1c_2$
J134427-103541	HE 1341-1020	2.35	1.915	$a_1a_3a_4a_5a_7f_1$	$a_1a_3a_4a_5a_7f_1f_2$
J012417-374423	Q 0122-380	1.91	0.822	$a_3a_5a_6a_7b_1c_1c_2$	$a_3a_5a_6a_7b_1c_1c_2$
J012417-374423	Q 0122-380	1.91	0.859	$a_3a_5a_6a_7b_1c_1c_2$	$a_5a_6a_7b_1c_1c_2$
J012417-374423	Q 0122-380	1.91	1.243	$a_2a_3a_4a_5b_1c_1e_1e_2$	$a_3a_4a_5c_1c_2$
J024008-230915	PKS 0273-23	2.23	1.635	$a_1a_3a_6b_1c_1c_2e_1e_2f_1$	$a_3a_6a_7c_1c_2f_1$
J024008-230915	PKS 0273-23	2.23	1.637	$a_1a_3a_6a_7b_1c_1c_2$	$a_1a_3a_6a_7c_1c_2$
J024008-230915	PKS 0273-23	2.23	1.657	$a_3a_5b_1c_2d_1f_1$	$a_3a_5d_1f_1$
J000344-232355	HE 0001-2300	2.28	0.452	$a_3a_5a_7b_1c_1c_2$	$a_4a_5a_7b_1c_1c_2$
J000344-232355	HE 0001-2300	2.28	2.185	-	$a_3a_4a_5c_1c_2d_1f_1$
J000344-232355	HE 0001-2300	2.28	2.187	-	$a_3a_4a_6c_2d_1f_1$
J011143-350300	Q 0109-3518	2.40	1.182	$a_3a_5a_7b_1c_1c_2$	$a_3a_5a_7b_1c_1c_2$
J011143-350300	Q 0109-3518	2.40	1.350	$a_3a_5a_6a_7b_1c_1c_2$	$a_3a_4a_5a_6a_7b_1d_1f_1$
J222006-280323	HE 2217-2818	2.41	0.942	$a_3a_5a_6a_7b_1c_1c_2$	$a_5a_7c_1c_2$
J222006-280323	HE 2217-2818	2.41	1.556	$a_3a_5a_6a_7c_1d_1$	$a_3a_5a_6a_7c_1c_2f_1$
J135038-251216	HE 1347-2457	1.44	1.439	$a_1a_2a_3c_1c_2f_2g_2i_1i_2i_3j_1j_2$	$a_3a_6f_1f_2$
J045523-421617	Q 0453-423	2.66	0.908	$a_3a_7b_1c_2$	$a_3a_5a_7c_1c_2$
J045523-421617	Q 0453-423	2.66	1.858	$a_3a_5a_7c_1d_1$	$a_3a_5a_7c_1c_2$
J000448-415728	Q 0002-422	2.76	1.542	$a_3a_4a_5a_7c_2$	$a_3a_5a_6a_7c_1c_2$
J000448-415728	Q 0002-422	2.76	2.168	$a_1a_3c_1c_2d_1f_1$	$a_1a_3a_5a_6a_7d_1f_1$
J000448-415728	Q 0002-422	2.76	2.302	$a_1f_1h_1h_2$	$a_1a_3a_5d_1f_1$
J212912-153841	PKS 2126-150	3.29	2.022	-	$a_3a_5a_6c_2f_1$

unity to still require a systematic, non-zero, error term to be applied to derive a more robust estimate of the error term of that weighted mean (see Table 4 and its footnote).

5 PROFILE FITTING ANALYSIS: BEST FITS

These absorption system models are our best Voigt profile fits to the data. The velocity structures for each absorption system in this model have been determined completely independently of those shown in C04.

5.1 Fitting regions

We choose fitting regions such that the flux recovers to the continuum and we include continuum regions either side of the absorption. Including ample continuum regions is important because: (i) if the model at the edge of the truncated region is significantly different from unity the convolution algorithm of VPFIT will not return a reliable flux estimate for the pixels near the truncated edge, (ii) it prevents the clipping of the wings of absorption features, assuring *all* parts of the absorption cloud are modelled, and (iii) we can allow for a varying continuum as an additional free parameter in the fit, if necessary.

5.2 Number of Voigt profile components used in a fit

We follow the fitting procedure described in King et al. (2012) to choose the optimal number of components in the fit. We use the Akaike Information Criterion (AIC) corrected for finite sample sizes (Sigiura 1978), defined as

$$AICc = \chi^2 + 2p + \frac{2p(p+1)}{(n-p-1)}, \quad (2)$$

where p is the number of free parameters and n is the number of data points included in a fit (Akaike 1974). We explore a range of models with different numbers of Voigt profile components, the adopted final model being the one with the smallest AICc. We only add a Voigt profile component to a fit if the addition of the component lowers the numerical value of the AICc. Employed this way, the AICc simply provides an additional check against fitting too many Voigt profile components to an absorption system.

5.3 Transitions used in a fit

For our best fits we attempted to fit all transitions that show absorption features, if possible. Occasionally ionic transitions part of absorption systems blend with features of interest in absorption systems from different redshifts. If this

Table 3. Results on $\Delta\alpha/\alpha$ for many-multiplet absorption system fits. Errors given are 1σ (σ_{stat}) and are taken directly from the covariance matrix diagonal terms (i.e. not corrected for random systematic effects). Column 2 lists the emission redshift, z_{em} , of the quasar. Column 3 lists the absorption system redshift, z_{abs} . Columns 4 and 5 list the χ^2_v , $\Delta\alpha/\alpha$ and associated error in units of 10^{-5} for our best fits to the absorption systems. Columns 6 and 7 list the same results for Variant I (C04 emulations) and columns 8 and 9 list the results for Variant II (restricted spectral fitting regions). We can predict the expected $\Delta\alpha/\alpha$ values for a given sight-line and model of α variation. Column 10 shows the predicted values of $\Delta\alpha/\alpha$ according to the King et al. (2012) dipole model $\Delta\alpha/\alpha = A\cos(\Theta) + m$. Absorption systems marked with an asterisk were not included in the analysis for our best fit and Variant II models (see Section 5.6).

Quasar Name	z_{em}	z_{abs}	Best fits		Variant I		Variant II		Dipole Prediction
			χ^2_v	$\Delta\alpha/\alpha[10^{-5}]$	χ^2_v	$\Delta\alpha/\alpha[10^{-5}]$	χ^2_v	$\Delta\alpha/\alpha[10^{-5}]$	$\Delta\alpha/\alpha[10^{-5}]$
J134427-103541	2.35	0.873	0.803	2.990 \pm 1.770	1.733	2.220 \pm 0.544	0.929	4.500 \pm 1.780	0.251
J134427-103541	2.35	1.278	0.827	0.337 \pm 1.130	3.797	3.900 \pm 1.140	1.187	0.438 \pm 1.130	0.251
J134427-103541	2.35	1.915	0.734	0.459 \pm 0.968	1.133	0.217 \pm 0.670	0.747	0.191 \pm 0.917	0.251
J012417-374423	1.91	0.822	0.794	0.923 \pm 1.090	1.035	1.220 \pm 1.100	1.047	1.210 \pm 1.100	0.145
J012417-374423	1.91	0.859	0.878	2.160 \pm 2.070	2.157	-1.850 \pm 0.936	1.864	2.000 \pm 1.970	0.145
J012417-374423	1.91	1.243	0.955	0.407 \pm 0.881	3.380	-1.180 \pm 1.080	1.147	1.300 \pm 0.935	0.145
J024008-230915	2.23	1.635	0.767	0.608 \pm 1.230	1.451	0.961 \pm 1.120	1.184	0.860 \pm 1.230	-0.180
J024008-230915	2.23	1.637	0.691	-0.237 \pm 1.180	1.985	0.496 \pm 0.772	0.688	-0.812 \pm 1.220	-0.180
J024008-230915	2.23	1.657	0.771	-0.958 \pm 1.300	1.468	0.766 \pm 0.555	0.834	-0.970 \pm 1.150	-0.180
J000344-232355	2.28	0.452	0.883	-0.706 \pm 0.713	2.883	-1.500 \pm 0.574	1.093	-0.803 \pm 0.690	0.071
J000344-232355	2.28	2.185*	N/A	N/A	0.832	7.090 \pm 1.990	N/A	N/A	0.071
J000344-232355	2.28	2.187*	N/A	N/A	1.139	-0.373 \pm 1.120	N/A	N/A	0.071
J011143-350300	2.40	1.182	0.806	0.298 \pm 0.965	0.792	0.217 \pm 0.974	0.696	0.048 \pm 0.925	0.124
J011143-350300	2.40	1.350	0.856	0.175 \pm 0.378	1.444	-2.030 \pm 0.959	1.020	-1.770 \pm 0.974	0.124
J222006-280323	2.41	0.942	0.947	0.686 \pm 1.130	2.480	-1.400 \pm 0.508	1.009	0.068 \pm 1.010	0.324
J222006-280323	2.41	1.556	1.059	1.050 \pm 0.520	2.132	1.260 \pm 0.508	1.078	1.760 \pm 0.666	0.324
J135038-251216	1.44	1.439	0.759	-0.071 \pm 0.404	3.452	-0.941 \pm 0.613	1.029	-0.607 \pm 0.297	0.444
J045523-421617	2.66	0.908	0.896	-1.240 \pm 0.540	5.577	-0.294 \pm 0.350	1.090	-1.330 \pm 0.553	0.044
J045523-421617	2.66	1.858	0.627	0.069 \pm 3.400	6.603	0.905 \pm 0.624	0.834	0.077 \pm 3.540	0.044
J000448-415728	2.76	1.542	0.759	-1.150 \pm 1.290	1.839	-4.400 \pm 0.753	0.560	-2.450 \pm 3.750	0.316
J000448-415728	2.76	2.168	0.709	1.640 \pm 1.350	3.181	0.477 \pm 0.416	1.294	1.580 \pm 1.380	0.316
J000448-415728	2.76	2.302	0.895	1.600 \pm 0.852	6.500	-0.356 \pm 0.621	1.352	-0.241 \pm 0.522	0.316
J212912-153841	3.29	2.022*	N/A	N/A	0.941	-1.490 \pm 1.260	N/A	N/A	0.257
$(\chi^2_v)_{mean}$			0.82		2.39		1.03		

contamination is severe, or if there is evidence for strong contamination by incompletely removed cosmic rays or telluric features, we remove those transitions from the analysis. Where this contamination is not severe we model the blended profiles with additional Voigt profile components.

In two cases we were able to identify the redshift, atomic species and wavelength of the blending (i.e. contaminating) transition. Absorption from Fe II λ 2382 in an absorption system at $z=1.542$ fell close enough to absorption caused by Mg II λ 2803 in the absorption system at $z=0.989$ in quasar J000448-415728. Also absorption from Mg II λ 2803 in an absorption system at $z=1.350$ fell close enough to absorption caused by Mg II λ 2796 in the absorption system at $z=1.343$ in quasar J011143-350300. In these cases we fitted both absorption systems simultaneously, increasing the information available to constrain both models. The simultaneous fitting was only required for the absorption systems in our best fits, as the contaminating features fell outside the spectral fitting regions of Variant II.

The actual transitions used in fitting each absorption system are listed in Table 2.

5.4 Thermal vs. turbulent fits

The line-widths for different species can be related turbulently or thermally. Previous analyses using the MM method have initially constructed Voigt profile fits to absorption systems using a wholly turbulent broadening mechanism (i.e. $b_{thermal} = 0$). Once the fit of an absorption system was complete, it was re-run using a wholly thermal broadening mechanism (i.e. $b_{turbulent} = 0$). As long as the values of $\Delta\alpha/\alpha$ did not differ by more than 1σ , the fit with the lowest χ^2 was chosen as the final fit (Webb et al. 1999; Murphy et al. 2004).

King et al. (2012) followed the same procedure in deriving first turbulent and then thermal fits, but then chose to implement a method-of-moments estimator that takes into account relative differences in the AICc of each fit, and the agreement, or otherwise, between the values of $\Delta\alpha/\alpha$.

We adopted a method of initially fitting all absorption systems as wholly turbulent. Later in the fitting process, when other ionic species were included in the fit, the line-broadening parameter was switched to wholly thermal in some cases in order to obtain a better model to the absorption system data. If and only if the AICc was reduced in the iteration after switching broadening mechanisms would

the thermal broadening mechanism be kept in further fitting iterations. For the 20 cases considered in our final fits, 15 were turbulent for our best fits and Variant II. All fits for Variant I were made using a wholly turbulent broadening mechanism (see Section 6.1).

As a consistency check, we also re-analysed all final fits using both broadening mechanisms as in Webb et al. (1999, 2001); Murphy et al. (2004). None of the fits re-analysed with the alternative broadening mechanism were found to have a lower AICc or χ^2 than the original broadening mechanism chosen.

5.5 General fitting procedure

We use VPFIT, a non-linear χ^2 minimization procedure, which requires the user to supply initial model parameters. We adopt the following systematic approach, as follows:

(i) The initial velocity structure is built up as a first guess using the strongest unsaturated transition. VPFIT then iterates to minimize χ^2 . This initial step is carried out with wholly turbulent line-broadening parameters. Additional components are added to improve the fit iteratively and Voigt profile components are only added if they reduce the AICc. We inspect the value of χ^2 , adding components such that $\chi^2_\nu \approx 1$.

(ii) Once a satisfactory fit to the first transition, by itself, is obtained, that velocity structure is applied to other transitions of the same species. For example, if the Mg II $\lambda 2796$ transition was the first one fitted, Mg II $\lambda 2803$ is now fitted simultaneously with Mg II $\lambda 2796$. The addition of components is repeated, as in (i).

(iii) We add transitions of different species to the fit, tying physically related parameters. For example, if Mg II $\lambda 2796$ and Mg II $\lambda 2803$ have been fitted, we now add all available Fe II transitions tying relevant parameters to the Mg II transitions. The exception to this is the Al III doublet. Where available, Al III is included in a simultaneous fit but without any tied N, b or z parameters, such that it contributes independently to estimates of $\Delta\alpha/\alpha$. The reason for not tying N, b, z is that its higher ionization potential may result in velocity segregation from the other species. The reason for inclusion is that the difference in q -coefficients of the Al III doublet (Table 1) are large (and different) enough to provide a useful additional sensitivity to a $\Delta\alpha/\alpha$ measurement.

(iv) In practice three things were taken into consideration in deciding upon the final model: χ^2_ν , the normalised residuals, and the AICc. For all final models, components are only added if they provide a reduction in the numerical value of the AICc, no obvious correlations remain in the normalised residuals, and χ^2_ν was close to unity.

(v) After a final best fit is attained we once again switch the line-broadening mechanism and inspect the AICc. In all cases switching the broadening mechanism after a final fit was attained resulted in an increased the AICc, therefore we kept the previous line-broadening mechanism for each fit.

The entire fitting process is carried out with $\Delta\alpha/\alpha$ set to zero. The introduction of $\Delta\alpha/\alpha$ as a free parameter is only done once the velocity profile/model to the absorption system has been finalised. Once a complete fit is attained VPFIT iterates one last time letting α vary as an additional free parameter.

An example fit is shown in the first column of Figure 1.

5.6 Systems rejected from analysis

5.6.1 Absorption system at $z_{abs} = 2.185 - 2.187$ along the line of sight to quasar J000344-232355

We attempted to fit the absorption complex from $z_{abs} = 2.185$ to $z_{abs} = 2.187$ as a single absorption system because of the proximity of the absorption features present at each redshift. The absorption features of Fe II $\lambda 2344$ at $\lambda 7471\text{\AA}$ and Fe II $\lambda 1608.45$ at $\lambda 5126.5\text{\AA}$ both exhibited a shift with respect to the corresponding absorption features present in the other transitions for this absorption system. We found no evidence for any contamination by identified or unidentified interlopers and the addition of components did not resolve the issue. We could not get a good model to the data and did not arrive at a final best fit. Since a best fit, with $\chi^2_\nu \approx 1$ and statistically acceptable normalised residuals, could not be attained, this system failed our consistency check and was rejected from our analysis.

5.6.2 Absorption system at $z_{abs} = 2.022$ along the line of sight to quasar J212912-153841

This system showed absorption by a Mg II doublet, Si II and multiple Fe II transitions. To provide an accurate measurement of $\Delta\alpha/\alpha$ one needs a set of transitions, that when analysed in combination, are sensitive to α variation. Fe II transitions have large, positive q -coefficients and Mg II/Si II have small q -coefficients (also known as “anchors”). The only anchor lines available in this absorption system are the Mg II doublet and a Si II $\lambda 1526$ line. The Mg II doublet falls in a part of the spectrum heavily contaminated by telluric lines at $\lambda \approx 8470\text{\AA}$. Si II $\lambda 1526$ falls within the Lyman- α forest, contaminated by intervening H I. Fe II $\lambda 1608$, which could potentially be used with the other Fe II transitions to constrain $\Delta\alpha/\alpha$ because of its large and negative q -coefficient, also falls within the forest. The only lines that are free of contamination are the remaining Fe II transitions, all of which have similar q -coefficients. We have therefore rejected this absorption system from our analysis.

5.7 Best fit results

Results of individual measurements of $\Delta\alpha/\alpha$, for each model, are provided in Table 3.

The weighted mean, using statistical errors only, for our best fits is $\Delta\alpha/\alpha = (0.165 \pm 0.174) \times 10^{-5}$, with $\chi^2_\nu = 1.10$. We apply the LTS method to the 20 absorption systems in our best fit model and find no outliers.

For our main result we find $\sigma_{rand} = 0.479 \times 10^{-5}$, a weighted mean and error on weighted mean of

$$\Delta\alpha/\alpha = (0.223 \pm 0.226) \times 10^{-5}, \quad (3)$$

with a χ^2_ν of 1.10. No outliers were found. Individual values of $\Delta\alpha/\alpha$ and robust 1σ error estimates (σ_{total}) are presented in Figure 2. The results of our best fitting model, using purely statistical errors (σ_{stat}), are presented in Figure 3 as black circles.

5.7.1 Comparison with Chand et al. (2004) and Srianand et al. (2007)

The absorption systems in our best fit model have been previously analysed by C04. They reported $\Delta\alpha/\alpha = -0.06 \pm 0.06 \times 10^{-5}$. Following a series of criticisms (Murphy et al. 2007, 2008), Srianand et al. (2007) revised the previous C04 result to $\Delta\alpha/\alpha = 0.01 \pm 0.15 \times 10^{-5}$, although not all criticisms were addressed in the revised analysis.

Our best fit results do not conflict with the mean $\Delta\alpha/\alpha$ value of the updated C04 analysis reported in Srianand et al. (2007). While our errors on the weighted mean are larger, and include a random systematic term, there is no conflict in the results. However, our analysis of model Variants I & II shows that there are significant systematic effects which remain unaccounted for in the C04 and Srianand et al. (2007) results (see Section 6).

5.7.2 Comparison with the King et al. (2012) dipole variation

In order to compare the results from our best fits with the possible dipole model reported by King et al. (2012), we proceed as follows. We calculate

$$\chi^2 = \sum_{i=1}^N \frac{(x_i - y_i)^2}{\sigma_i^2}, \quad (4)$$

where x_i is the i th measurement of $\Delta\alpha/\alpha$ for our best fits, y_i is the corresponding value of $\Delta\alpha/\alpha$ predicted for that position in the sky according to the dipole model parameters found in King et al. (2012) and σ_i is the 1σ statistical uncertainty associated with that measurement from our best fit results. For the dipole model of $\Delta\alpha/\alpha = A \cos(\Theta) + m$ we use the parameters reported in King et al. (2012) of angular amplitude $A = 0.97^{+0.22}_{-0.20} \times 10^{-5}$, pointing in the direction $RA = (17.3 \pm 1.0)\text{hr}$, $dec = (-61 \pm 10)^\circ$ and having a monopole term of $m = (-0.18 \pm 0.08) \times 10^{-5}$.

Following King et al. (2012) we also use the LTS method to calculate σ_{rand} for our best fit results with respect to the dipole model and use this value as a measure of scatter with respect to the dipole model.

We find a $\chi^2_\nu = 0.99$ for our best fits with respect to the dipole model. Using the LTS method we calculate $\sigma_{rand} = 0.434 \times 10^{-5}$. Comparing these values to those calculated with respect to a weighted mean, $\chi^2_\nu = 1.10$ and $\sigma_{rand} = 0.479 \times 10^{-5}$, we find that the data do not conflict with the dipole results reported in King et al. (2012).

To make a direct comparison with the weighted mean calculations in Table 4, we adopt the dipole parameters above and calculate the expected values of $\Delta\alpha/\alpha$ for each data point in the best fit sample. For these expected dipole values of $\Delta\alpha/\alpha$ we take the errors from our best fits, that is, the statistical errors on each point returned by VPFIT. The expected weighted mean for this sample is $(\Delta\alpha/\alpha)_I = (0.205 \pm 0.174) \times 10^{-5}$. These results agree with the statistical analysis of Kraiselburd et al. (2014) who found general consistency between the results of Murphy et al. (2003), King et al. (2012) and Srianand et al. (2007).

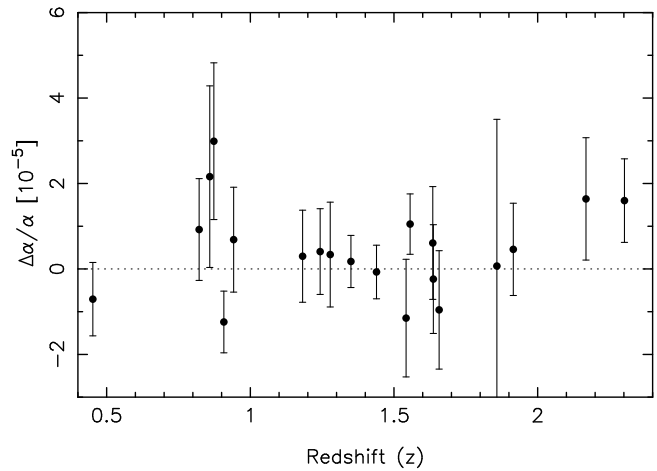


Figure 2. Results from our best fits after increasing error bars on individual measurements of $\Delta\alpha/\alpha$. 1σ errors shown are $\sigma_{total}^2 = \sigma_{stat}^2 + \sigma_{rand}^2$. The weighted mean for this analysis is $\Delta\alpha/\alpha = (0.223 \pm 0.226) \times 10^{-5}$.

6 COMPARISON OF DIFFERENT FITTING METHODOLOGIES

We employ three different fitting methodologies, which we name our best fits, Variant I and Variant II. By modelling the absorption systems in different ways we are able to compare modelling techniques and their effect on the measurement of the variation of α and associated errors. Our best fits have been discussed previously. Variant I employs the fitting approach of C04 and Variant II mimics a very specific aspect of the C04 Voigt profile fitting methodology. Details of each model, and common methods, are provided in the following subsections.

6.1 Variant I: Under-fitting with restricted fitting regions

In this model we emulate the Voigt profile fitting procedure used by C04. Murphy et al. (2008) have demonstrated that absorption systems that are fit with too few Voigt profile components, as is the case for the C04 analysis, will produce spurious results of $\Delta\alpha/\alpha$. To examine if these fitting choices have an effect on the measurement of $\Delta\alpha/\alpha$ and errors we have used the model parameters, transitions and fitting regions listed in C04 as a basis for Variant I. That is, we have used z and b components provided in their analysis as starting guesses. The b -parameters, z 's and transitions used in a fit are provided in C04. However the column densities and fitting ranges are not provided directly in C04. Column density starting guesses were chosen by fixing all parameters in an absorption system except column densities, and letting VPFIT iteratively find a χ^2 minimum for the column densities alone. All fits for Variant I use the turbulent line broadening mechanism. We have used the same spectra, extractions, error arrays and atomic data as were used for our best fit models. We employ VPFIT as our χ^2 minimization algorithm.

This model differs from our best fits in many important respects:

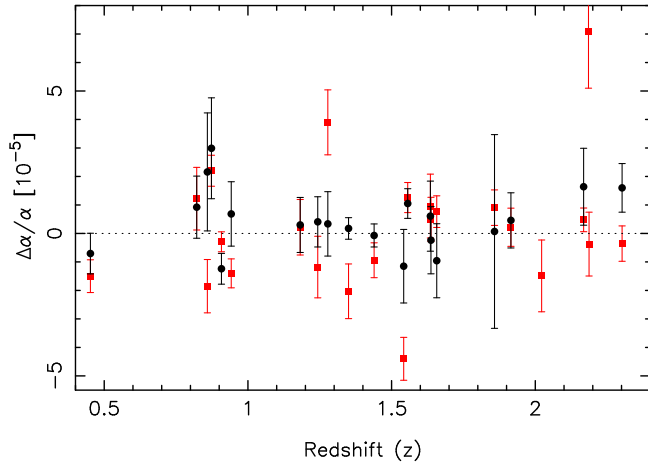


Figure 3. Results from our best fitting model (black circles) are compared with results of Variant I (red squares). All errors shown are 1σ and purely statistical (σ_{stat}). Note the increased scatter of Variant I values of $\Delta\alpha/\alpha$, as is clear from the plot and the values of χ^2_ν for each fit (see Figure 7). For our best fits, only taking into account raw statistical errors, $\chi^2_\nu = 1.10$ for the weighted mean. For Variant I, only taking into account raw statistical errors, $\chi^2_\nu = 5.11$ and the weighted mean is $\Delta\alpha/\alpha = (-0.047 \pm 0.138) \times 10^{-5}$.

(i) Wavelength ranges are restricted so as to only include the strongest parts of absorption, sometimes so much so that little or no continuum regions are included. This means that parts of the absorption system that affect the model are neglected (for example, see Figure 1, the feature at -35 km s^{-1} in Mg II $\lambda 2796$ and Mg II $\lambda 2803$ in Variant I). Specifically, spectral fitting regions were chosen to match those present in the plots provided in C04.

(ii) In many cases, our best fits make use of ionic transitions that are excluded from Variant I. These are generally transitions that show weak absorption. An example of this is illustrated in Fig. 1, where we include an Mg I transition in our best Voigt profile fit. The statistical impact of including all possible transitions is small but generally helps to improve the accuracy of the $\Delta\alpha/\alpha$ measurement, as we demonstrate in Section 6.3.3.

(iii) Table 2 shows that 27 of the transitions included in Variant I fits are not included in our best fits. In all excluded cases, this is because close inspection reveals problems such as blending with atmospheric absorption features or contamination by unidentified absorption that could not be adequately modelled. The inclusion of contaminated transitions has the potential to produce spurious results of $\Delta\alpha/\alpha$. An example of this is the absorption system at $z_{abs} = 1.556$ towards quasar J222006-280323, Si II $\lambda 1526$ absorption is blended with Lyman forest absorption and Mg II $\lambda 2803$ absorption is blended with the O_2 band.

(iv) The vast majority of fits in Variant I contain far fewer parameters than the fits for our best model, i.e. Variant I is under-fit, as has been demonstrated in Murphy et al. (2008). This also has potential to produce spurious results of $\Delta\alpha/\alpha$.

An example fit of Variant I is shown in column two of Figure 1.

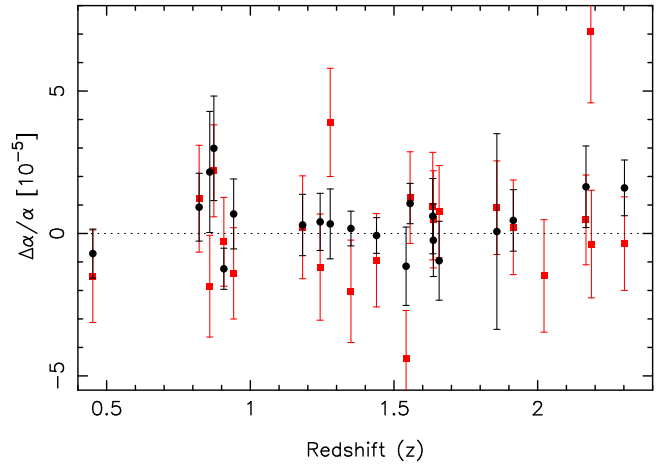


Figure 4. Comparison between our best fitting model (black circles) and Variant I (red squares) after increasing error bars on individual results of $\Delta\alpha/\alpha$. 1σ errors shown are $\sigma_{total}^2 = \sigma_{stat}^2 + \sigma_{rand}^2$. The weighted mean for Variant I using statistical and systematic errors is $\Delta\alpha/\alpha = (0.002 \pm 0.361) \times 10^{-5}$ with $\chi^2_\nu = 1.22$.

6.2 Variant II: Restricted spectral fitting regions

We have opted to include a third modelling technique to investigate the effects of a specific aspect of fitting present in C04. Variant II is the same as our best fits in all respects except one; the spectral fitting regions are reduced to exactly match those of C04. Modelling in this manner allows us to quantitatively investigate the effects of reduced spectral fitting regions on $\Delta\alpha/\alpha$ and associated errors by a comparison of our best fits with Variant II. We use the same Voigt profile fits, spectra, error arrays and atomic data as are used for our best fits. The only change is the spectral fitting regions. Where a Voigt profile component does not fall within the chosen fitting regions, we do not use that component in our fit. Spectral fitting regions are adjusted and components falling outside those regions dropped. VPFIT iterates a new minimum of χ^2 and a new value of $\Delta\alpha/\alpha$ and associated error.

An example of a Variant II absorption system is shown in column three of Figure 1.

6.3 Results for Variants I and II

6.3.1 Variant I: Under-fitting with restricted fitting regions

The weighted mean, using statistical errors only, for Variant I is $\Delta\alpha/\alpha = (-0.047 \pm 0.138) \times 10^{-5}$, with $\chi^2_\nu = 5.11$. We apply the LTS method to the 23 absorption systems in Variant I and find no outliers. These data points are presented in Figure 3 as red/grey squares.

Allowing for non-zero σ_{rand} , we find $\sigma_{rand} = 1.519 \times 10^{-5}$, a weighted mean and error on weighted mean of

$$\Delta\alpha/\alpha = (0.002 \pm 0.361) \times 10^{-5}, \quad (5)$$

with a χ^2_ν of 1.22. No outliers were found. Individual values of $\Delta\alpha/\alpha$ and robust 1σ error estimates (σ_{total}) are presented in Figure 4 as red/grey squares.

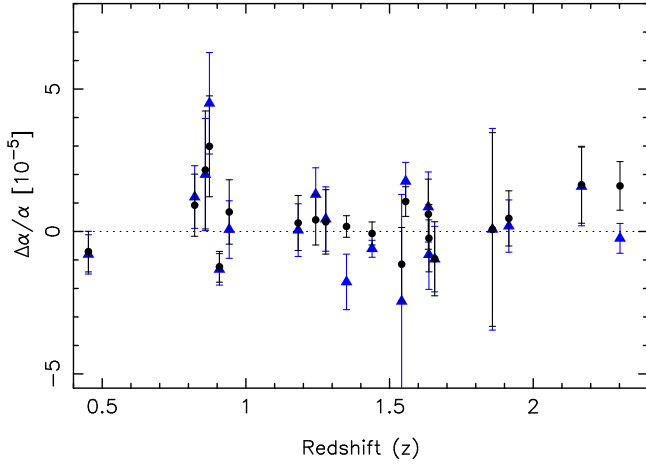


Figure 5. Comparison between our best fit results (black circles) and Variant II results (blue triangles). All errors shown are 1σ and purely statistical (σ_{stat}), derived solely from the relevant covariance matrix diagonal terms calculated by VPFIT. For Variant II, only taking into account raw statistical errors, $\chi^2_\nu = 1.83$ and the weighted mean is $\Delta\alpha/\alpha = (-0.200 \pm 0.174) \times 10^{-5}$. While Variant II does show an increase in the scatter of individual values of $\Delta\alpha/\alpha$, both models are in good agreement with each other.

6.3.2 Variant II: Reduced spectral fitting regions

The weighted mean, using statistical errors only, for Variant II is $\Delta\alpha/\alpha = (-0.200 \pm 0.174) \times 10^{-5}$, with $\chi^2_\nu = 1.83$. We apply the LTS method to the 20 absorption systems in Variant II and find no outliers. These data points are presented in Figure 5 as blue/grey triangles.

Allowing for non-zero σ_{rand} , we find $\sigma_{rand} = 0.970 \times 10^{-5}$, a weighted mean and error on weighted mean of

$$\Delta\alpha/\alpha = (0.107 \pm 0.319) \times 10^{-5}, \quad (6)$$

with a χ^2_ν of 0.79. No outliers were found. Individual values of $\Delta\alpha/\alpha$ and robust 1σ error estimates (σ_{total}) are presented in Figure 6 as red/grey squares.

6.3.3 Quantifying the effect of reduced spectral fitting regions

The only differences between the modelling techniques of our best fits and those of Variant II are the sizes of the spectral fitting regions chosen for the fits. Voigt profile components that fall outside these regions are necessarily excluded. The vast majority of these Voigt profile components are weak components falling on the outskirts of the main, stronger features of the absorption system. In some cases strong absorption features are ignored due to the choice of fitting regions, such as the absorption features at $v \approx -50 \text{ km s}^{-1}$ in the middle panel of Figure 1. By comparing the results of our best fits with those of Variant II we can directly test the effect of reduced spectral fitting regions on the determination of $\Delta\alpha/\alpha$. Table 4 lists the weighted means with purely statistical errors and also the weighted means that have accounted for extra scatter by increasing the 1σ error bars via σ_{rand} .

Figure 5 shows a plot of results comparing our best fit results with those of Variant II. Overall, there is good

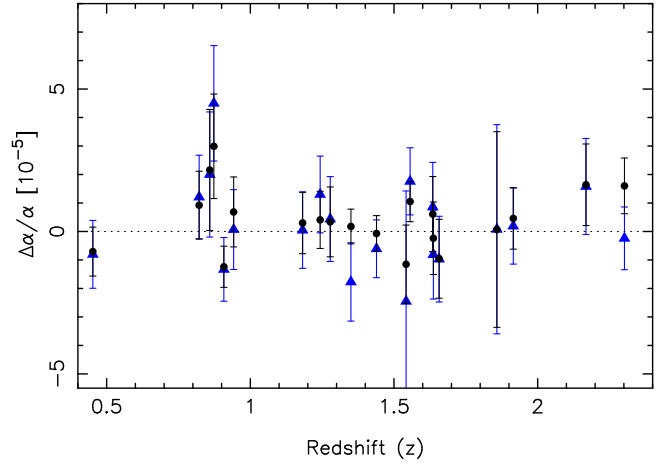


Figure 6. Comparison between our best fit results (black circles) and Variant II results (blue triangles) after increasing error bars on individual results of $\Delta\alpha/\alpha$. 1σ errors shown are $\sigma_{total}^2 = \sigma_{stat}^2 + \sigma_{rand}^2$. The weighted mean for Variant I using statistical and systematic errors is $\Delta\alpha/\alpha = (0.107 \pm 0.319) \times 10^{-5}$ with $\chi^2_\nu = 0.79$.

agreement. $\Delta\alpha/\alpha$ values generally agree very well between both models, although there is more scatter for the Variant II points.

We note that our best fit absorption systems at $z_{abs} = 1.542$ and $z_{abs} = 1.350$ are contaminated by intervening absorption systems that reside in different redshifts, and happen to fall on that part of the spectrum (these absorption systems and their parameter values can be viewed supplementary material). The absorption system towards J000448-415728 at $z_{abs} = 1.542$ was fitted simultaneously with another at $z_{abs} = 1.989$ because the transition Mg II $\lambda 2803$ in the latter blends with Fe II $\lambda 2383$ in the former. Also the absorption system towards at $z_{abs} = 1.350$ was fitted simultaneously with a magnesium doublet at $z_{abs} = 1.344$ because the Mg II $\lambda 2803$ transition in the latter blends with Mg II $\lambda 2796$ in the former. Systems $z_{abs} = 1.542$ and $z_{abs} = 1.350$ are *not* treated as contaminated in Variant II, as the wavelength fitting ranges are restricted enough so as to exclude the contaminating absorption features. Therefore it is inappropriate to compare the results of our best to the Variant II results for absorption systems $z_{abs} = 1.542$ and $z_{abs} = 1.350$.

6.3.4 Extra scatter when fitting regions are restricted

As previously discussed, we calculate the error on each $\Delta\alpha/\alpha$ measurement as a quadrature addition of two terms (Section 4), one derived from the covariance matrix at the best fit, σ_{stat} , the other allowing for additional sources of error such as velocity structure ambiguities, calibration and other uncertainties, σ_{rand} . Since our best fit model and Variant II are identical in fitting methodology apart from a variation of fitting regions, the comparison between the two models can be parametrized in terms of σ_{rand} . If restricting the fitting region has the effect of increasing the scatter on $\Delta\alpha/\alpha$ measurements this would be indicated as an associated increase in σ_{rand} .

Because of the two systems removed, as discussed in

the previous section, there are 18 points common to both samples. The result for our best fits is

$$(\sigma_{rand})_{Best} = 0.457 \times 10^{-5} \quad (7)$$

for 18 absorption systems. The result for Variant II is

$$(\sigma_{rand})_{II} = 0.867 \times 10^{-5} \quad (8)$$

for 18 absorption systems. We see an $\approx 90\%$ increase in σ_{rand} for Variant II over our best fits. Since the only difference between the two models is the choice of fitting regions, this extra scatter exhibited by Variant II is a direct consequence of restricting spectral fitting regions. This result illustrates the necessity of careful choice of fitting regions and the significance to which poor choice of fitting regions can lead to spurious measurements of $\Delta\alpha/\alpha$.

The increase in σ_{rand} due to narrow fitting regions is perhaps at first sight surprising. However, Figure 1 illustrates the reason. It can be seen that for Variant II, the relatively strong absorption seen in Mg II for velocities less than about -25 km s^{-1} must impact on the stronger components at velocities immediately to the right of -25 km s^{-1} . In turn, modifications in the range $-25 \text{ km s}^{-1} < v < 0 \text{ km s}^{-1}$ will have a knock-on effect further into the complex, and so on. Including the full fitting range allows VPFIT to properly evaluate redshift parameter errors. However, if a narrow fitting range is used, VPFIT is “tricked” into computing artificially small redshift errors. Figure 5 and 6 illustrate further the consequence of inappropriately narrow fitting regions. The blue triangles (Variant II) exhibit greater scatter than the black points.

6.3.5 Quantifying the effect of excluding weak transitions from a fit

The measurement of $\Delta\alpha/\alpha$ is of course most sensitive to strong, unsaturated, absorption features. We have used transitions that show relatively weak absorption features. This is justified by the fact that the statistical uncertainty of the fits using these transitions is improved, albeit marginally.

For example, Variant I does not include three weakly absorbing transitions (Mg I $\lambda 2852$ and Fe II $\lambda 2344/2587$) in the fit of the absorption system at $z_{abs} = 0.942$ along the line of sight to quasar J222006-280323 (see Variant I in Figure 1). In our best fits to the data we include these transitions (see our best fit in Figure 1) and find $\Delta\alpha/\alpha = (0.686 \pm 1.130) \times 10^{-5}$ for this system. Removing Mg I $\lambda 2852$ and Fe II $\lambda 2344/2587$ from the fit and re-calculating $\Delta\alpha/\alpha$ we find $\Delta\alpha/\alpha = (0.627 \pm 1.390) \times 10^{-5}$. There is an increase in the uncertainty of $\Delta\alpha/\alpha$ when these weak transitions are removed and the value of $\Delta\alpha/\alpha$ does not significantly change.

Another example is the absorber at $z_{abs} = 1.637$ along the line of sight to quasar J024008-230915. For our best fit of this absorber $\Delta\alpha/\alpha = (-0.237 \pm 1.180) \times 10^{-5}$. Variant I excludes the weakest transition in this absorption system, Mg I $\lambda 2852$. Removing this transition from our best fit and re-calculating $\Delta\alpha/\alpha$ we find $\Delta\alpha/\alpha = (-0.253 \pm 1.200) \times 10^{-5}$.

The two examples above show that, for these particular cases, when fitting multiple transitions in the same species, including the weakest transitions or transition causes the 1σ error estimate on $\Delta\alpha/\alpha$ to reduce by about 10%. The actual

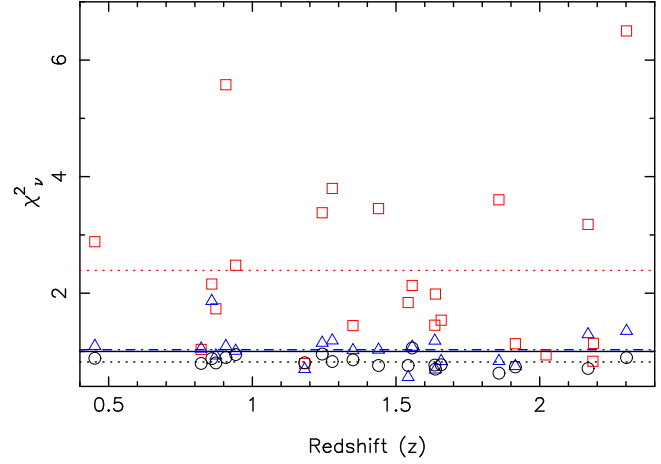


Figure 7. χ^2_ν comparison. Black circles show individual values for our best fit results, red squares show individual values for Variant I and blue triangles show individual values for Variant II. Black dotted line, red dotted line and blue dash-dotted line show the means of $(\chi^2_\nu)_{Best} = 0.82$, $(\chi^2_\nu)_I = 2.39$ and $(\chi^2_\nu)_{II} = 1.03$, for our best fits, Variants I and II respectively. Our best fits and Variant II show very few points in excess of unity, suggesting that the absorption systems are statistically acceptable fits for these models. Variant I shows many points with values of χ^2_ν well in excess of unity, suggesting that these models are not statistically good fits to the data.

value of $\Delta\alpha/\alpha$ shifts by a negligible amount compared to the 1σ error estimate. We have not attempted to generalise this further, although one would expect it to be beneficial to include *all* transitions of all strengths for a given species in cases like this, where stronger lines in that species are clear detections.

6.3.6 Quantifying the effect of under-fitting

The fitting methodology of Variant I differs from that of our best fits in three important respects, *i*) differences in spectral fitting regions, *ii*) differences in transitions included in a fit, and *iii*) differences in modelling of velocity structure, that is, Variant I uses fewer velocity components, even after allowing for the restricted spectral fitting regions. Here, by comparing our best fits with Variant I, and noting of the effects of points *i*) and *ii*) above, we show that under-fitting has the most significant (and adverse) impact on estimating $\Delta\alpha/\alpha$.

Comparing overlapping fitting regions between our best fit model with Variant I, i.e. comparing like with like, the AICc method results (our best fits) in a 60% increase in the number of components compared to the Variant I model. For example, compare the middle panel (Variant I) and the third panel (Variant II) in Figure 1. Variant II contains twice as many velocity components as Variant I. The mean χ^2_ν for Variant I is $(\chi^2_\nu)_{mean} = 2.39$, reflecting the fact that Variant I does not, in general, attain statistically acceptable fits to absorption systems. Figure 7 shows a comparison of the values of χ^2_ν for each individual absorption system for all three models.

Table 4. Summary and comparison of results for the 23 absorption systems studied in this work. Column 1 enumerates the different results. Column 2 gives descriptions of the sample. Column 3 gives the number of absorption systems analysed in each sample. Column 4 gives χ^2_ν for each sample. Column 5 gives the weighted mean and 1σ uncertainty of each sample, in units of 10^{-5} . Column 6 shows the raw statistical error on the weighted mean and column 7 shows σ_{rand} as calculated by the LTS method. Rows 1-3 only show statistical 1σ uncertainties (σ_{stat}). Rows 4-6 show robust error estimates, estimated by increasing uncertainties by adding a constant in quadrature to match the scatter (σ_{total}).

I	Sample	N_{abs}	χ^2_ν	$\Delta\alpha/\alpha[10^{-5}]$	$\sigma_{stat}[10^{-5}]$	$\sigma_{rand}[10^{-5}]$
1	Best fits: Optimal fits, statistical errors	20	1.10	0.165 ± 0.174	0.174	-
2	Variant I: C04 emulations, statistical errors	23	5.11	-0.047 ± 0.138	0.138	-
3	Variant II: Restricted fitting regions, statistical errors	20	1.83	-0.200 ± 0.174	0.174	-
4	Best fits - Robust errors	20	0.77 ^a	0.223 ± 0.226	0.174	0.479
5	Variant I - Robust errors	23	1.22 ^a	0.002 ± 0.361	0.138	1.519
6	Variant II - Robust errors	20	0.79 ^a	0.107 ± 0.319	0.174	0.970

^aNote the expectation values of χ^2_ν are not unity. The LTS method we have used produces robust error estimates by estimating the additional σ_{rand} term from a fraction ($f = 0.85$ in our case) of the entire sample such that the observed scatter about the weighted mean matches the theoretical expectation for that subset. To illustrate this, the theoretical expectation of χ^2_ν for our best fits, when LTS is applied to a subset of the entire sample (17 data points in this case), is 0.44. σ_{rand} is derived by matching the observed and theoretical χ^2_ν . The σ_{rand} derived in this way is then applied to the *whole* sample.

6.3.7 Extra scatter in Variant I

We further quantify the effect of under-fitting on the data by comparing the value of σ_{rand} for each model. We follow the same procedure as in Section 6.3.4. We also only calculate σ_{rand} for a subset of systems that are common to both our best fits and Variant I. The result for our best fits is

$$(\sigma_{rand})_{Best} = 0.457 \times 10^{-5} \quad (9)$$

for the 18 systems that are in common. The result for Variant I is

$$(\sigma_{rand})_I = 1.300 \times 10^{-5}. \quad (10)$$

We therefore see from the above, and from Section 6.3.4, that compared to independent fits, restricting the fitting regions (Variant II) increases σ_{rand} by from 0.457×10^{-5} to 0.867×10^{-5} , and under-fitting further increases σ_{rand} from 0.867×10^{-5} to 1.300×10^{-5} , i.e. both fitting choices have a significant adverse effect on the fitting accuracy.

6.3.8 Effect of under-fitting on σ_{stat} and σ_{rand}

A well-known feature of non-linear least-squares modelling is that parameter error estimates derived from the covariance matrix at the best-fit solution (as is done by VPFIT) are only reliable when a number of conditions are met, one of which is that the model is a statistically valid representation of the data. If this is not the case, one would not expect a non-linear least-squares procedure to return meaningful parameters and parameter errors.

Inspecting Table 3, comparing our best fit results with those of Variant I, it can be seen that in some cases our best fits yield substantially larger error estimates than Variant I (C04). However, in other cases, the error estimates are seen to be in good agreement. In a few cases, the error estimate we derive from our best fits are actually smaller than those for Variant I. The explanations for this are as follows. Our best fits contain, on average, a higher number of velocity components than Variant I. When close blending occurs in the transitions most sensitive to an alpha variation, i.e. the stronger, often central components, we clearly

expect a substantial increase in the $\Delta\alpha/\alpha$ error estimate. On the other hand, when the additional components fall sufficiently far from the main components determining alpha, little difference is expected between the best fit and Variant I $\Delta\alpha/\alpha$ error estimates. Finally, because our best fits include additional transitions not used in Variant I, and when the additional velocity components do not fall in the stronger lines, we expect the best fit $\Delta\alpha/\alpha$ error estimates to reduce compared to Variant I.

The following example illustrates a substantial result of under-fitting exhibited within this dataset. We can isolate the impact of under-fitting the data by comparing Variants I and II and use, as an example, the $z_{abs} = 0.942$ system towards J222006-280323 (shown in Figure 1) to illustrate the problems. Figure 1 and Table 2 show that for this system, our best fits included 3 additional weak transitions Mg I $\lambda 2852$, Fe II $\lambda 2586$ and Fe II $\lambda 2344$. To directly assess the impact of under-fitting alone, and using our best fit as a template, we re-fit this system excluding those transitions and adopting the restricted wavelength fitting regions of Variant I. The results for the re-fit are $\Delta\alpha/\alpha = (-0.047 \pm 1.140) \times 10^{-5}$. When including the 3 weak transitions, our original Variant II result gave $\Delta\alpha/\alpha = (0.068 \pm 1.010) \times 10^{-5}$. Variant I, which now comprises exactly the same transitions and fitting regions gives $\Delta\alpha/\alpha = (-1.400 \pm 0.508) \times 10^{-5}$. The uncertainties quoted here are statistical only, i.e. the errors returned provided by VPFIT. The Variant I errors are a factor of two too small and the actual $\Delta\alpha/\alpha$ value for Variant I differs significantly from our best fit value.

The problems caused by under-fitting are highlighted further still when one considers the scatter in the sample as a whole. The Variant I sample exhibits far more scatter about a mean value than Variant II (red squares in Figure 6). The values of σ_{rand} for the Variant I and II samples are 1.688×10^{-5} and 0.916×10^{-5} respectively. Using the example absorption system from the previous paragraph, if we now attempt to estimate a random systematic error term we find that it has ballooned for Variant I, due to the excess scatter present in the data. The final error estimate,

including statistical and random systematic terms added in quadrature, for absorption system $z_{abs} = 0.942$ for Variant I is 1.602×10^{-5} , while it is only 1.227×10^{-5} for our best fit. This example highlights two important, albeit subtle, considerations. First, under-fitting results in meaningless parameter errors. Second, under-fitting results in greater scatter overall.

7 CONCLUSIONS

Our work investigates profile fitting methodologies and provides a new analysis of 23 quasar absorption systems. Our findings are as follows:

(i) It is important to use a reproducible and systematic approach to estimating the number of absorbing components fitted to an absorption complex. Here we have used the AICc statistic to estimate the number of components required. Our best fits, on average, use $\approx 60\%$ more Voigt profile components to adequately model an absorption region of the same size as Variant I. When an insufficient number of components are used to model an absorption system the numerical value of $\Delta\alpha/\alpha$ changes significantly (i.e. the value of σ_{rand} is much smaller for the ensemble of our best fits compared to Variant I - see Section 6.3.6). The larger number of components results in a much smaller scatter amongst an ensemble of $\Delta\alpha/\alpha$ estimates. Also, the increased number of components means more model parameters which in turn causes the estimated statistical uncertainty on $\Delta\alpha/\alpha$ to increase, as one would expect. Conversely, underestimating the number of free parameters in the model produces a significantly smaller estimated uncertainty on $\Delta\alpha/\alpha$, but if the model is incorrect, both parameter estimates and associated errors are meaningless. Figure 1 gives a strong example of this: for that absorption system our best fit gives a result of $\Delta\alpha/\alpha = (0.686 \pm 1.130) \times 10^{-5}$ and the Variant I model's results are $\Delta\alpha/\alpha = (-1.400 \pm 0.508) \times 10^{-5}$.

(ii) When modelling absorption features, it is important that fitting regions cover all relevant parameters, including continuum regions without detectable absorption. Put differently, it is important to avoid subjective selection of what may appear to be the “most interesting” or strongest features. It is incorrect to assume that weaker absorption features nearby have an insignificant impact on the best-fit model parameters and their associated errors. Restricting fitting regions in this way (our Variant II model) produces a 90% increase in σ_{rand} when compared to the results of our best fit model.

(iii) Combining the impact of both restricted fitting regions and under-fitting results in an increase of the error estimate on the weighted mean of the sample of 60% when compared to our best fit model.

(iv) Using our robust error estimates, we find a final weighted mean our independent analysis of the Chand et al. (2004) dataset (our best fits) of $\Delta\alpha/\alpha = (0.223 \pm 0.226) \times 10^{-5}$. The weighted mean of our best fits, quoting statistical errors only, is found to be $\Delta\alpha/\alpha = (0.165 \pm 0.174) \times 10^{-5}$.

(v) Our best results are also consistent with the dipole model of α variation presented in King et al. (2012).

(vi) The analysis of our best fits to the absorption systems are consistent with the weighted mean of the much larger

sample of 154 absorption systems analysed by King et al. (2012) of $\Delta\alpha/\alpha = (0.208 \pm 0.124) \times 10^{-5}$.

ACKNOWLEDGEMENTS

We are grateful to the referee, Paulo Molaro, for very helpful comments which significantly improved the manuscript. We would like to thank R. F. Carswell and J. C. Berengut for advice and insightful comments on early version of the manuscript. M. T. Murphy thanks the Australian Research Council for Discovery Project grant DP110100866 which supported this work. M. R. Wilczynska has been supported in part by an Australian Postgraduate Award.

REFERENCES

- Akaike A., 1974, IEEE Trans. Automat. Contr., 19
- Chand H., Srianand R., Petitjean P., Aracil B., 2004, A&A, 417, 853
- Dirac P. A. M., 1937, Nature, 139
- Dumont V., Webb J. K., 2016, MNRAS, in preparation
- Dzuba V. A., Flambaum V. V., Webb J. K., 1999, Phys. Rev. Lett., 82, 888
- Eddington A., 1931, Proc. Camb. Philos. Soc., 27
- Evans T. M., Murphy M. T., Whitmore J. B., Misawa T., Centurion M., D’Odorico S., Lopez S., Martins C. J. A. P., Molaro P., Petitjean P., Rahmani H., Srianand R., Wendt M., 2014, MNRAS, 445, 128
- Griest K., Whitmore J. B., Wolfe A. M., 2010, ApJ, 708
- King J. A., Mortlock D. J., Webb J. K., Murphy M. T., 2009, Memorie della Società Astronomica Italiana, 80
- King J. A., Webb J. K., Murphy M. T., Flambaum V. V., Carswell R. F., Bainbridge M. B., Wilczynska M. R., Koch F. E., 2012, MNRAS, 422, 3370
- Kraisselburd L., Landau S., Simeone C., 2014, Mem. S.A.It., 85, 102
- Molaro P., Levshakov S. A., Monai S., Centurion M., Bonifacio P., D’Odorico S., Monaco L., 2008, A&A, 481, 559
- Murphy M. T., Flambaum V. V., Webb J. K., Dzuba V. A., Prochaska J. X., Wolfe A. M., 2004, LNP, 648
- Murphy M. T., Tzanavaris P., Webb J. K., Lovis C., 2007, MNRAS, 378, 221
- Murphy M. T., Webb J. K., Flambaum V. V., 2003, MNRAS, 345
- Murphy M. T., Webb J. K., Flambaum V. V., 2007, Phys. Rev. Lett., 99, 239001
- Murphy M. T., Webb J. K., Flambaum V. V., 2008, MNRAS, 384, 1053
- Murphy M. T., Webb J. K., Flambaum V. V., Curran S. J., 2003, AP&SS, 283
- Rahmani H., Wendt M., Srianand R., Noterdaeme P., Petitjean P., Molaro P., Whitmore J. B., Murphy M. T., Centurion M., Fathivavsari H., D’Odorico S., Evans T. M., Levshakov S. A., Lopez S., Martins C. J. A. P., Reimers D., Vladilo G., 2013, MNRAS, 435, 861
- Rousseeuw P. J., 1984, Amer. Statistical. Assoc., 79
- Rousseeuw P. J., Driessen K., 2006, Data Min. Knowl. Discov., 12, 29
- Sigiura N., 1978, Commun. Stat. A-Theor., 7

- Srianand R., Chand H., Petitjean P., Aracil B., 2007, *Phys. Rev. Lett.*, 99, 239002
- Uzan J., 2011, *Living Rev. Rel.*, 14
- Webb J. K., Flambaum V. V., Churchill C. W., Drinkwater M. J., Barrow J. D., 1999, *Phys. Rev. Lett.*, 82
- Webb J. K., King J. A., Murphy M. T., Flambaum V. V., Carswell R. F., Bainbridge M. B., 2011, *Phys. Rev. Lett.*, 107
- Webb J. K., Murphy M. T., Flambaum V. V., Dzuba V. A., Barrow J. D., Churchill C. W., Prochaska J. X., Wolfe A. M., 2001, *Phys. Rev. Lett.*, 87
- Weyl H., 1919, *Ann. Phys.*, 59
- Whitmore J. B., Murphy M. T., 2015, *MNRAS*, 447, 446